Sedanolide alleviates LPS-induced depressive-like behaviors by modulating the C3a/C3aR signaling axis and microglial glycolysis

SHAOCONG LU*, FANGLA LUO*, NIQI CHEN, GONGDE SHI and YERU CHEN

Department of Anesthesiology, Sir Run Run Shaw Hospital, School of Medicine, Zhejiang University, Hangzhou, Zhejiang 310016, P.R. China

Received January 29, 2026; Accepted July 3, 2026

DOI: 10.3892/mmr.2026.13967

Abstract. A total of ~30% of patients with depression do not respond to pharmacological treatment. Sedanolide (SD) is a compound derived from Chinese medicinal herbs and has structural features associated with anti-inflammatory activity. However, its effect on depressive disorders remains unclear. The present study aimed to examine the therapeutic effects of SD in lipopolysaccharide (LPS)-induced depressive disorder and to investigate the underlying mechanisms. An LPS-induced male mouse model of depressive-like behavior was used to evaluate the therapeutic effect and underlying mechanisms of SD. The mRNA levels of pro-inflammatory cytokines and the activation state of microglia in the medial prefrontal cortex (mPFC) were assessed. In addition, high-throughput RNA sequencing was performed as an unbiased transcriptomic screen to identify differentially expressed genes. Western blotting and ELISA assays were then used to validate the expression and activation levels of key candidate molecules within the identified pathways. BV-2 cell line was utilized to assess the aerobic glycolysis *in vitro* by metabolic extracellular flux analysis. Finally, the selective C3aR antagonist SB290157 was administered to determine whether the effects of SD depended on the downstream C3a/C3aR signaling cascade. SD treatment significantly increased the sucrose preference and reduced immobility time in both the tail suspension test and the forced swimming test in LPS-treated mice. Mechanistically, SD attenuated LPS-induced neuroinflammation and microglial activation in the mPFC. High-throughput RNA sequencing identified C3 and matrix metalloproteinase-9 as key transcriptional targets potentially involved in the effects of SD. Crucially, both *in vitro* and *in vivo* ELISA assays revealed that SD directly suppressed complement C3 activation by inhibiting its proteolytic cleavage into the active C3a fragments. Furthermore, SD reduced abnormal microglial aerobic glycolysis and restored mitochondrial respiration *in vitro*. By contrast, pharmacological inhibition of C3aR completely abolished protective effects of SD on behavioral despair, anhedonia, neuroinflammation and metabolic reprogramming. These findings indicate that SD alleviates depressive-like behaviors. The C3a/C3aR signaling axis appears to play a critical role in mediating its anti-inflammatory and anti-glycolytic effects.

Correspondence to: Dr Yeru Chen, Department of Anesthesiology, Sir Run Run Shaw Hospital, School of Medicine, Zhejiang University, 3 Qingchun East Road, Hangzhou, Zhejiang 310016, P.R. China
E-mail: yeruchen@zju.edu.cn

*Contributed equally

Key words: depressive disorder, sedanolide, complement C3, microglia

Introduction

Major depressive disorder (MDD) is a common psychiatric disorder characterized by persistent low mood, a loss of interest or pleasure in previously enjoyable activities, and recurrent thoughts of death. According to the World Health Organization, >300 million people worldwide experience a form of depression to varying degrees, representing ~20% of the population and imposing a substantial socioeconomic burden (1). Since Smith first proposed the neuroinflammation hypothesis of depression in 1991 (2), accumulating evidence has highlighted a critical role for neuroinflammation in the pathophysiology of depression. The prefrontal cortex, particularly the medial prefrontal cortex (mPFC), plays a central role in social cognition and socio-emotional processing (3). Lipopolysaccharide (LPS)-induced inflammation reduces the number of GABAergic interneuron in the mouse hippocampus and prefrontal cortex (4).

Microglia are the primary immune sentinels of the central nervous system and contribute to neuronal homeostasis, immune surveillance, and the resolution of inflammatory responses (5). Preclinical studies have shown that intraperitoneal administration of LPS induces IL-1β cleavage and increases the expression of nod-like receptor pyrin domain-containing 3 (NLRP3) in the hippocampus (6). Immunofluorescence analyses further demonstrated that NLRP3 expression is predominantly localized to Iba-1 positive microglia compared with control animals. Therefore, microglial activation in the mPFC represents an important target for investigating the mechanisms underlying LPS-induced depressive-like behavior. Accordingly, suppressing neuroinflammation and limiting

microglial activation may represent effective strategies for alleviating depression.

The complement system is a critical component of innate immunity that facilitates the recognition, surveillance, and clearance of exogenous and endogenous danger signals derived from pathogens or damaged and dying cells, including pathogen-associated molecular patterns and damage-associated molecular patterns (7). Complement C3 serves as the central convergence point of the complement cascade and integrates the three major complement activation pathways. Activation of these pathways generates, C3 convertases, which cleave C3 into C3a and C3b, two key-mediators of immune activation and neuroinflammation (8). Previous studies have shown that C3 deficiency in neuron-glial cultures and mouse brains significantly attenuates LPS-induced oxidative damage and neurodegeneration (9). Although C3/C3aR signaling has traditionally been viewed as a pro- inflammatory pathway, emerging evidence suggests that it also regulates cellular metabolism (10,11). Notably, C3ar1-deficient microglia exhibit resistance to metabolic alterations induced by hypoxia mimetics and display reduced expression of hypoxia-inducible factor-1 α (HIF-1α) (12).

Current antidepressant therapies are largely based on the monoamine hypothesis. However, ~20-30% of patients with depression fail to respond adequately to pharmacological treatment. Consequently, recent drug discovery efforts have focused on identifying novel antidepressant agents, particularly nutritional supplements and traditional herbal medicines, because of their favorable safety profiles, improved tolerability and reduced adverse effects (13). Sedanolide (SD) ($C_{12}H_{18}O_2$; PubChem CID, 5018391) also known as 5-butyl-3-hydroxy-2(5H)-furanone, is a naturally occurring compound found in several Umbelliferae species and traditional Chinese medicinal plants, including *Ligusticum chuanxiong* Hort., *Cnidium monnieri* (L.) Cuss., and *Apium graveolens* L (14). The structural feature comprises the double ring fusion of γ-lactone (A ring) and benzene (B ring), demonstrating notable anti-inflammatory properties and antioxidant properties (15). Studies have shown that supercritical carbon dioxide extracts of Chuanxion from volatile oil, which contain 6.31% SD, significantly improve cognitive function and reduce infarct volume in cerebral ischemia-reperfusion injury models. These neuroprotective effects are associated with reduced levels of nitric oxide and malondialdehyde, along with increased superoxide dismutase activity (16). In addition, SD enhances cell viability and acts as a novel natural inhibitor of human monoamine oxidase B in 6-hydroxydopamine-induced SH-SY5Y cell injury models (17). SD also markedly attenuates colonic inflammation by reducing the mRNA expression of pro-inflammatory cytokines, including IL-1β, IL-6 and TNF-α (18). Based on these findings, it was hypothesized that SD may alleviate LPS-induced neuroinflammation. In the present study, it was revealed that SD ameliorates LPS-induced depressive-like behaviors. Furthermore, the present results demonstrated that the inhibitory effects of SD on inflammatory response and aerobic glycolysis in microglial cells are critically dependent on the C3a/C3aR signaling axis. Together, these findings identify that SD as a potential therapeutic candidate for the treatment of neuroinflammation-associated depressive-like behaviors.

Materials and methods

Reagents. LPS (Escherichia coli O55:B5; purity ≥97%, purified by phenol extraction; specific activity ≥500,000 EU/mg) was obtained from Beijing Solarbio Science & Technology Co., Ltd. (cat. no. L8880), was diluted in sterile phosphate-buffered saline (PBS) to prepare the stock solution of the 10 mg/ml concentration and stored at -20˚C.

Animals. All animal experiments were performed in strict accordance with the laboratory animal testing guidelines of Zhejiang University and the Guide for the Care and Use of Laboratory Animals published by the National Institutes of Health. The primary experimental protocols were reviewed and approved by the Laboratory Animal Welfare and Ethics Review Committee, Zhejiang University (Hangzhou, China; approval no. ZJU20220307). The supplementary *in vivo* receptor-antagonism control procedures (LPS+SB290157 cohort) were independently authorized and approved by Animal Experimental Ethical Inspection of the Sir Run Run Shaw Hospital, Zhejiang University School of Medicine (Hangzhou, China; approval no. SRRSH2026-0041). The 6-week-old mice (weight, 20-22 g) were provided by Zhejiang Vital River Laboratory Animal Technology Co., Ltd. Alongside a 12/12-h light/dark cycle, the trial maintained a consistent temperature of 22˚C. A standard animal care facility supplied food and water for the mice throughout the week. The fewest number of animals possible were employed to minimize their suffering.

Animal treatment. A total of 144 male C57BL/6 mice were successfully utilized, evaluated, and euthanized in the present study, with zero premature mortality recorded. Pre-defined humane endpoints were established based on rigorous animal welfare criteria, including a body weight loss exceeding 20%, severe prolonged lethargy, or visible respiratory distress; notably, no animals reached these thresholds during the experimental timelines. The dosage and pre-treatment timeline of SD were selected based on previous *in vivo* studies (18) and optimized through preliminary pilot experiments. The *in vivo* phase comprised two distinct procedural blocks: i) The primary therapeutic evaluation cohort, wherein mice received daily intragastric gavage of SD (20 mg/kg) or vehicle for 8 consecutive days starting 3 days prior to a 5-day daily lipopolysaccharide (LPS; 1 mg/kg, i.p.) challenge (19,20), followed by sequential behavioral testing spanning 11 days; and ii) the C3aR inhibition paradigm, where animals were pre-treated with the selective C3aR antagonist SB290157 trifluoroacetate (30 mg/kg, i.p.) every alternate day beginning 2 days prior to any other interventions, followed by an 8-day concurrent SD/LPS regimen and a subsequent 9-day behavioral assessment matrix. At the scheduled experimental endpoints, deep anesthesia was initiated via the inhalation of 4% isoflurane inside a dedicated induction chamber for rapid induction and subsequently maintained at 2% isoflurane during the procedural verification. Anesthetic depth was strictly validated by the complete loss of the pedal withdrawal (toe-pinch) reflex prior to the procedure. Humane euthanasia was sequentially executed via cervical dislocation under this deep anesthetic state. Absolute death was clinically verified by the permanent

cessation of cardiac impulses and respiratory movements prior to anatomical tissue harvesting.

To optimize the preventative timing of SD prior to acute LPS challenge, a preliminary pilot study was conducted utilizing smaller animal cohorts (n=3-4 mice per group) using 19 mice. The protective phenotypes were systematically evaluated when mice were administered with SD (20 mg/kg, i.g.) daily for either 1, 2, or 3 consecutive days before the acute systemic challenge, which was subsequently maintained throughout the 5-day repetitive LPS regimen. Pilot behavioral observations indicated that a 3-day pre-treatment regimen offered the most stable, robust, and statistically significant positive effects in safeguarding against LPS-driven behavioral deficits compared with the 1- or 2-day groups. The results of preliminary pilot behavior tests were presented in Fig. S1.

Open field test (OFT). The OFT was conducted following established protocols (21). Prior to the studies, mice were acclimatized to the testing environment and lighting conditions for 30 min. Each mouse was individually placed in a square arena (dimensions: 45x45x45 cm^3) and allowed to explore freely for 15 min. After each test, the open field arena was sanitized with 75% ethanol. The locomotor and exploratory behaviors of the mice were recorded using ANY-maze software during the test.

Elevated plus maze (EPM). The EPM test was conducted following previously established techniques (21). The maze consisted of two open arms and two closed arms, elevated above the floor. Mice were placed individually at the center of the maze, facing one of the open arms, and their physical activity was recorded for a period of 5 min. Before testing the next mouse, the maze was cleaned with 75% ethanol. The movements of the mice were tracked and measured using ANY-maze software.

Marble burying test. The buried marble test relies on documenting the number of marbles buried at the end of the experiment. The test was originally designed to assess anxiety-like behavior. It is conducted in a polypropylene mouse cage measuring 42x24x12 cm, which has a metal grid on the top. The floor of the cage is covered with 5 cm of sawdust, and 20 clean glass marbles (1.5 cm in diameter) are evenly distributed across the surface. During the test, the marbles are arranged with uniform spacing. Mice are placed in this enclosure for 30 min. ~24 h after initial training on the testing day, 15 marbles are distributed evenly within the test cage. The mice are exposed to the marbles for 3 min while being recorded on video. The number of buried marbles is subsequently calculated.

Tail suspension test (TST). The TST was conducted as outlined in previous research (22). ~1/3 of the mouse's tail was secured and suspended from a base, with the head positioned 20 cm above the ground. Animal activity was recorded from a lateral perspective. The mice were suspended for a total of 6 min, during which an observer, unaware of the treatment the animals received, timed their immobility during the last 4-min assessment. Animals were deemed motionless when they exhibited no body movements and remained passively suspended.

Forced swimming test (FST). The mice were placed in a glass chamber (35 cm in height, 30 cm in diameter) filled with warm water. The water temperature was maintained between 22 and 24˚C, with a depth of 20 centimeters. The water depth was calibrated to prevent the animals from contacting the substrate using their tails or hind limbs. Animal behaviors were recorded via videotape from a lateral perspective. The rodents were allowed to swim freely for 6 min, and an observer blinded to the treatment conditions recorded the duration of the immobility during the final 4-min assessment. Immobility was defined as the time when the animals remained stationary or afloat, displaying only the movements necessary to maintain their balance in the water.

Sucrose preference test (SPT). The mice were housed individually and acclimated with two bottles of water for two days, followed by two bottles of 2% sucrose for another two days. After a period of 24 h without water, the mice were provided with one bottle of 2% sucrose and one bottle of water for 2 h during the dark phase. During the 2-h test, the positions of the bottles were swapped after 1 h. The total consumption of each fluid was recorded, and sucrose preference was determined by calculating the average sucrose consumption ratio over the first 2 h. The sucrose intake ratio was computed by dividing total sucrose consumption by the combined intake of water and sucrose.

Reverse transcription-quantitative PCR (RT-qPCR). Total RNA was extracted from the mPFC using the FastPure Cell/Tissue Total RNA Extraction Kit V2 (Vazyme Biotech Co., Ltd.). The quality and quantity of the RNA were assessed with a NanoDrop spectrophotometer (Thermo Fisher Scientific, Inc.). Subsequently, cDNA was synthesized from the RNA using the First Strand cDNA Synthesis Kit (Monad Biotech Co., Ltd.) according to the manufacturer's instructions. qPCR was then performed using SYBR Green I (Foregene Co., Ltd) on an A&B Applied Biosystems device. The thermocycling conditions were as follows: Initial denaturation at 95˚C for 30 sec, followed by 40 cycles of denaturation at 95˚C for 10 sec and annealing/extension at 60˚C for 30 sec. The expression levels of the target genes were normalized to GAPDH using the $2^{-\Delta\Delta Cq}$ approach (23). The nucleotide sequences of the primers used in RT-qPCR were: TNF-α forward, 5'-CCC TCACACTCAGATCATCTTCT-3' and reverse, 5'-GCTACG ACGTGGGCTACAG-3'; IL-6 forward, 5'-TAGTCCTTC CTACCCCAATTTCC-3' and reverse, 5'-TTGGTCCTTAGC CACTCCTTC-3'; IL-1β forward, 5'-GCAACTGTTCCTGAA CTCAACT-3' and reverse, 5'-ATCTTTTGGGGTCCGTCA ACT-3'; LCN2 forward, 5'-TGGCCCTGAGTGTCATGTG-3' and reverse, 5'-CTCTTGTAGCTCATAGATGGTGC-3'; C3 forward, 5'-CCAGCTCCCCATTAGCTCTG-3' and reverse, 5'-GCACTTGCCTCTTTAGGAAGTC-3'; S100a8 forward, 5'-AAATCACCATGCCCTCTACAAG-3' and reverse, 5'-CCC ACTTTTATCACCATCGCAA-3'; matrix metalloproteinase-9 (MMP9) forward, 5'-CTGGACAGCCAGACACTAAAG-3' and reverse, 5'-CTCGCGGCAAGTCTTCAGAG-3'; Itgal forward, 5'-CCAGACTTTTGCTACTGGGAC-3' and reverse, 5'-GCTTGTTCGGCAGTGATAGAG-3'; Clec14a forward, 5'-CTTCACCACGCTACCTTCAAG-3' and reverse, 5'-AAA CCCCTTAAAGGCTCTTTCTC-3'; Myo1g forward, 5'-GGC

CCTGAGTATGGGAAACC-3' and reverse, 5'-GATACGAGC ACCTCACCAATG-3'; Cybb forward, 5'-TGTGGTTGGG GCTGAATGTC-3' and reverse, 5'-CTGAGAAAGGAGAGC AGATTTCG-3'; Frg forward, 5'-CGGCTGAAGAACGCT ATTACC-3' and reverse, 5'-GGGCGACGAATATGGTCA CTC-3'; Adh1 forward, 5'-GCAAAGCTGCGGTGCTATG-3' and reverse, 5'-TCACACAAGTCACCCCTTCTC-3'; GAPDH forward, 5'-AGGTCGGTGTGAACGGATTTG-3' and reverse, 5'-GGGGTCGTTGATGGCAACA-3'.

Western blot analysis. Mice were subjected to deep anesthesia and subsequently processed according to a previously established methodology (24) to obtain mPFC tissue. After homogenizing the tissues in ice-cold RIPA Lysis and Extraction buffer (cat. no. 89900; Thermo Fisher Scientific, Inc.) solution containing PMSF, they were centrifuged for 15 min at 4˚C at 11,200 x g. The BCA assay (cat. no. P0011; Beyotime Institute of Biotechnology) was utilized to measure concentrations following the manufacturer's instructions. Equal amounts of protein (20 μg per lane) were separated on 4-20% gradient SDS-polyacrylamide gels. SDS-PAGE was performed to separate the proteins, which were then transferred to PVDF membranes. The primary antibodies used included LCN2 (1:1,000; cat. no. A2092), Itgal (1:1,000; cat. no. A23960), Complement C3 (1:1,000; cat. no. A26625PM), MMP9 (1:1,000; cat. no. A0289) and β-actin (1:3,000; cat. no. AC026; all from ABclonal Biotech Co., Ltd.). These antibodies were incubated on membranes with 5% non-fat milk in PBST (0.1% Tween-20) for 1 h at room temperature, followed by overnight incubation at 4˚C. The membranes were then allowed to equilibrate at room temperature for 1 h while being treated with the appropriate secondary antibodies (Goat anti-Rabbit IgG (H+L) Secondary Antibody, HRP: 1:5,000; catalog no. 31460; Thermo Fisher Scientific, Inc.; and Goat anti-Mouse IgG (H+L) Secondary Antibody, HRP: 1:5,000; catalog no. 31430; Thermo Fisher Scientific, Inc.). Super ECL Detection Reagent (catalog no. 36208ES76; Shanghai Yeasen Biotechnology Co., Ltd.) was employed for visualization, and images were captured using the ChemiDoc Touch Imaging System (Bio-Rad Laboratories, Inc.). Band intensities were analyzed using ImageJ software (version 1.54p; National Institutes of Health).

Immunostaining. In accordance with the methodology detailed in previous studies, serial cryostat sections with a thickness of 25 μm were prepared (15,16). The sections underwent treatment with 5% donkey serum (catalog no. 36136ES60; Shanghai Yeasen Biotechnology Co., Ltd.) and 0.3% Triton X-100 for 1 h at room temperature. This was followed by overnight incubation at 4˚C with an antibody diluent containing goat antibodies against Iba-1 (1:200; cat. no. ab178846; Abcam). Subsequently, the sections were washed with PBS at three 10-min intervals. After washing, they were incubated at room temperature for 1 h with Alexa Fluor 594 goat anti-rabbit antibody (1:1,000; catalog no. ab150080; Abcam). Fluorescent images were captured using a Nikon A1 confocal microscope. Image acquisition was conducted using Image-Pro Plus 5.0 software (Media Cybernetics, Inc.), ensuring that all parameters remained consistent throughout the process.

Morphometric analysis for microglia. The approach (25) was followed to conduct a morphometric evaluation of the microglia. High-resolution images with distinct cellular architecture were obtained using confocal fluorescence microscopy (Nikon Corporation). To analyze the target region layer by layer, an x40 objective was employed. Additionally, multi-plane virtual-Z mode was used to reconstruct the cellular architecture in three dimensions after the analysis. At least five $Iba1^+$ cells were present in each location, and 10 images of individual microglia were captured from each mouse studied. Following the examination of the images, skeletonization was performed using ImageJ's skeleton analysis. The terminal positions of the microglia were counted, and the maximal branch length of the microglia was determined. Sholl analysis was conducted on binary images by utilizing the Sholl analysis tools available in ImageJ. An assessment of the cellular complexity was carried out by counting the number of intersections where concentric circles overlapped.

BV-2 cell culture. The BV-2 cell line, obtained from OriCell, was cultured in DMEM basic (1X) media (cat. no. C11995500BT; Gibco; Thermo Fisher Scientific, Inc.) supplemented with 10% fetal bovine serum (FBS; catalog no. A5209402; Gibco; Thermo Fisher Scientific, Inc.) and 1% penicillin/streptomycin (cat. no. 240004004; Beijing Solarbio Science & Technology Co., Ltd.) in a humidity-controlled incubator at 37˚C with 5% CO_2.

BV-2 cell treatment. The BV-2 cell line, maintained under optimal conditions, was inoculated into multi-well plates. The experiment began once the cells reached ~70-80% confluence in medium devoid of FBS. The cells underwent pre-treatment with SD (50 μM) for 2 h. Following pre-treatment, LPS (100 ng/ml) was immediately added to the culture medium for stimulation. Regarding SB290157 trifluoroacetate treatment, either dimethyl sulfoxide (DMSO) or 10 μM SB290157 was introduced to the BV-2 cell 1 h prior to the administration of SD (26). Cells were harvested 6 h after stimulation for RT-qPCR assays. Samples were collected 24 h after treatment for western blot analysis and metabolic extracellular flux assays.

For the concentrate of C3a by ELISA assay BV-2 microglial cells were cultured until achieving ~70-80% confluence, after which the culture medium was replenished with serum-free medium. To evaluate the regulatory effect of SD on complement C3 cleavage, cells were pre-treated with SD (50 μM) for 2 h. A total of 1 h prior to LPS stimulation, recombinant full-length mouse C3 protein (2 μg/ml; cat. no. HY-P78247; MedChemExpress) was introduced into the medium as an exogenous substrate. Subsequently, cells were administrated with LPS (100 ng/ml) to initiate the complement activation cascade. Following a 24-h incubation period, the cell culture supernatants were meticulously collected and centrifuged at 1,000 x g for 10 min at 4˚C to remove cellular debris. The concentration of active C3a fragment in the clarified supernatants was quantitatively determined using a commercial Mouse C3a Enzyme-Linked Immunosorbent Assay (ELISA) kit according to the manufacturer's instructions. Concurrently, the adherent cells were washed with ice-cold PBS and lysed using RIPA buffer. The total protein concentration of each well was measured via a BCA protein assay kit.

BV-2 microglial cells were cultured until achieving ~70-80% confluence, after which the culture medium was replenished with serum-free medium. Cells were pre-treated with SD (50 μM) for 2 h. A total of 1 h prior to LPS stimulation, recombinant mouse C3a protein (1 μg/ml; cat. no. HY-P7863; MedChemExpress) was introduced into the medium. Subsequently, cells were administrated with LPS (100 ng/ml) to initiate the inflammation activation cascade. Following a 24-h incubation period, the whole cell harvested and lysed using RIPA buffer. The total protein concentration of each well was measured via a BCA protein assay kit.

Estimating metabolic extracellular flux. The ideal cell density was selected, and the experiments were conducted (27). Quadruplicates or quintuplicates of BV-2 cell lines were cultured on XF-96 plates with LPS and SD. Microglia were washed and assessed in XF Running buffer A (10 mM glucose, 1 mM sodium pyruvate, and 2 mM L-glutamine) for oxygen consumption rate (OCR) or extracellular acidification rate (ECAR) at designated intervals. Measurements were received in real-time before and after pharmacological interventions, including the MitoStress assay with 1 μM oligomycin, 1 μM FCCP and 1 μM rotenone, as well as the glycolysis stress experiment with 10 mM glucose, 1 μM oligomycin, and 50 mM 2-DG. When glucose was supplemented, ECAR measures reflected the basal ECAR, while OCR measures indicated the basal OCR. The difference between basal OCR and the peak OCR following FCCP treatment represented mitochondrial respiration capacity and ATP production. Glycolytic reserve (GR) was calculated as the difference between basal and peak ECAR after oligomycin administration.

Next generation sequencing. The RNA-Seq investigation involved collecting mPFC tissues harvested from the CTRL (n=4), LPS (n=5), SDN (n=5) and LPS+SDN (n=5) groups. The RNA sequencing process encompasses several key steps: Extracting RNA, constructing a library, sequencing, checking quality, mapping reads, analyzing differential expression, and performing functional enrichment. Following the manufacturer's instructions, TRIzol® Reagent was utilized to extract total RNA from the tissue samples. Subsequently, the 5300 Bioanalyzer (Agilent) was employed to assess the purity of the RNA, while the ND-2000 (NanoDrop Technologies; Thermo Fisher Scientific, Inc.) was used for quantification. For sequencing library creation, only RNA samples meeting strict quality criteria (OD260/280=1.8- 2.2, OD260/230 ≥2.0, RIN ≥6.5, 28S:18S ≥1.0,>1 μg) were selected. RNA purification, reverse transcription, library building, and sequencing were performed by Shanghai Majorbio Bio-pharm Biotechnology Co., Ltd. in accordance with the manufacturer's guidelines (Illumina, Inc.). The Illumina® Stranded mRNA Prep, Ligation from (Illumina, Inc.) was used to generate the mPFC RNA-seq transcriptome library. A total of 1 μg of total RNA for the experiment. The polyA selection method was employed with oligo(dT) beads to isolate messenger RNA, which was subsequently fragmented using a fragmentation buffer. Following this, the SuperScript double-stranded cDNA synthesis kit (Invitrogen; Thermo Fisher Scientific, Inc.) was used to generate double-stranded cDNA with random hexamer primers (Illumina, Inc.). In accordance with Illumina's library construction protocol, the synthesized cDNA was subjected to end repair, phosphorylation, and the addition of an 'A' base. Libraries were then size-selected for cDNA target fragments of 300 bp using 2% low-range ultra-agarose. Next, the fragments were amplified by PCR with Phusion DNA polymerase (New England BioLabs, Inc.) for 15 cycles. After quantification with the Qubit 4.0, the paired-end RNA-seq sequencing library was sequenced on the NovaSeq 6000 sequencer, which produces reads of 2x150 bp. The raw paired-end readings were reduced and fastp was used with the default settings to assess their quality. Subsequently, HISAT2 software (28) was employed to align the cleaned reads to the reference genome in oriented mode. StringTie (29) was utilized to generate mapped reads for each sample in a reference-based manner. To identify differentially expressed genes (DEGs) across two distinct samples, we quantified the expression level of each transcript using the transcripts per million reads methodology. RSEM was employed to measure gene abundances (30). For the differential expression analysis, either DESeq2 (31) or DEGseq (32) were used. DEGs were identified with $|\log_2 FC|>1$ and a false discovery rate (FDR) ≤0.05 using DESeq2, or with an FDR <0.001 using DEGseq. Additionally, functional enrichment analysis was performed, including Gene Ontology (GO) and Kyoto Encyclopedia of Genes and Genomes (KEGG) pathways, to identify DEGs that were significantly enriched in GO terms and metabolic pathways, with a Bonferroni-corrected P≤0.05 compared with the whole transcriptome background. GOATOOLS (https://github.com/tanghaibao/goatools) was used for GO functional enrichment analysis, and KOBAS (http://kobas.cbi.pku.edu.cn) was used for KEGG pathway analysis.

Mouse C3a ELISA assays. The concentration of active C3a fragment in the clarified supernatants was quantitatively determined using a commercial Mouse C3a ELISA kit (cat. no. NBP2-70037; Novus Biologicals, LLC) according to the manufacturer's instructions. To ensure experimental rigor and eliminate variations in cell density, the absolute concentrations of C3a obtained from the ELISA were normalized against the total protein content of the respective cell lysates and expressed as pg/mg total protein.

Statistical analysis. All data were collected and analyzed blindly. Data are presented as the mean ± SEM. Single comparisons were determined using a two-tailed Student's t-test. Two-way ANOVA with Tukey's multiple comparisons test was applied for multiple comparisons. Sample sizes were based on our previous study and relevant literature to ensure reliable measurements. Statistical analyses were conducted using GraphPad Prism 8.0 (GraphPad Software; Dotmatics). P<0.05 was considered to indicate a statistically significant difference. All statistical analyses are detailed in the figure legends and Table SI.

Results

SD alleviates LPS-induced depressive disorder. Adult wide-type C57BL/6 mice received with LPS (1 mg/kg) daily for 5 consecutive days. Mice were pretreated with SD (20 mg/kg, i.g.) for 3 days before LPS administration and

continued to receive SD for a total of 8 consecutive days (Fig. 1A). LPS treatment reduced body weight compared with the sham group, whereas SD significantly increased body weight in LPS-treated mice (Fig. 1B). Neither LPS nor SD affected locomotor activity, as indicated by the absence of significant differences in the total distance traveled during the OFT (Fig. 1C). Similarly, no significant difference was observed in the center time of the OFT test or in the time spent in the open arms of the EPM test among the experimental groups (Fig. 1C-E). The number of buried marbles also remained unchanged across all four groups (Fig. 1F). These findings indicate that neither LPS nor SD induced anxiety-like behavior. In the SPT, LPS-treated mice exhibited a significant reduction in sucrose preference, indicating the development of anhedonia-like behavior. SD treatment markedly increased the sucrose preference in the LPS-treated mice (Fig. 1G). In addition, LPS administration significantly increased immobility time in both the TST and FST compared with the control groups, indicating the induction of depressive-like behaviors. SD treatment effectively reversed these behavioral deficits (Fig. 1H and I). Collectively, these results demonstrate that SD alleviates LPS-induced depressive-like behaviors.

SD releases LPS-induced inflammatory responses. To evaluate the effects of SD on LPS-induced neuroinflammation, the mRNA expression levels of the pro-inflammatory cytokines, tumor necrosis factor α (TNF-α), interleukin-6 (IL-6) and interleukin-1β (IL-1β) were measured in the mPFC. RT-qPCR analysis showed that the mRNA levels of TNF-α, IL-6 and L-1β were significantly increased in the LPS-treated mice compared with sham mice controls (Fig. 2A). SD treatment led to a substantial reduction of these inflammatory cytokines in LPS-treated mice (Fig. 2A). To further examine microglial activation, morphometric analyses of microglia were performed in the mPFC. The representative images of immunofluorescence of Iba1 were shown in Fig. 2B. LPS-treated mice exhibited increased soma size and greater maximum branch length, morphological features indicative of microglial activation. SD treatment significantly attenuated these changes (Fig. 2C and D). Together, these results demonstrate that SD suppresses LPS-induced neuroinflammatory responses and microglial activation in the mPFC.

mRNA profile of SD on the LPS-induced mice. The prefrontal cortex, particularly the mPFC, plays a critical role in social cognition and socio-emotional processing (3). To examine the transcriptional changes associated with the effects of SD on LPS-induced depressive-like behaviors, high-throughput RNA sequencing of the mPFC was performed as an unbiased transcriptomic screening approach to identify DEGs. The DEG analysis identified 468 genes that were significantly altered between the LPS + SDN mice and LPS groups using a cutoff value of a fold change >2.0 and $P<0.05$. Among these genes, 22 were upregulated and 438 were downregulated. Compared with the CTRL group, LPS treatment increased the expression of 686 genes and decreased the expression of 29 genes in the mPFC. By contrast, comparison of the SDN and CTRL groups identified 107 altered genes, including 21 upregulated and 86 downregulated genes (Fig. 3A). The heatmap analysis revealed marked alterations in the mPFC transcriptomic profile following LPS treatment, whereas SD largely reversed the LPS-induced upregulation of gene expression (Fig. 3B). Consistently, the Venn diagram showed an overlap between genes upregulated in the LPS versus CTRL comparison and genes downregulated in the LPS + SDN versus LPS comparison (Fig. 3C). KEGG pathway enrichment analysis of the 120 overlapping genes provided preliminary insight into the molecular pathways underlying the effects of SD on LPS-induced depressive-like behaviors. Enriched pathways included 'Neutrophil extracellular trap formation', 'Cell adhesion molecules', 'Neuractive ligand-receptor interaction' and 'Coronavirus disease' (Fig. 3D). GO analysis further indicated enrichment in biological processes and cellular components related to 'Leukocyte migration', 'Positive regulation of response to external stimulus', 'Leukocyte cell', 'Collagen' and 'Regulation of cell' (Fig. 3E). These findings suggest that immune- and inflammation-related pathways contribute to the protective effects of SD against LPS-induced depressive-like behaviors.

Elevated C3 and MMP9 are involved in the effect of SD on the LPS-induced depressive-like behaviors. To further validate the transcriptomic findings, the 10 most significantly altered DEGs among the 120 overlapping genes identified in the mPFC were examined using RT-qPCR. LPS treatment significantly increased the mRNA level of LCN2, C3, S100a8, MMP9, Itgal, Myo1g, Cybb and Fgr. SD treatment significantly reduced the mRNA levels of LCN2, C3, Itgal and MMP9 in LPS-treated mice (Fig. 4A). The protein expression of LCN2, C3, Itgal and MMP9 was next assessed by western blot analysis. Among these candidates, C3 and MMP9 protein levels were significantly elevated following LPS administration. SD treatment effectively suppressed the LPS-induced upregulation of both C3 and MMP9 (Fig. 4B and C). These unbiased transcriptomic analyses identified C3 and MMP9 as key candidate targets associated with the effects of SD.

The consistent changes observed at both the mRNA and protein levels further support the involvement of C3 and MMP9 in the protective actions of SD against LPS-induced pathological alterations.

Role of SD on inflammation and aerobic glycolysis in BV-2 cell lines. To further validate the RNA-sequencing results, an *in vitro* BV-2 microglial cell model was established and the effects of LPS and SD treatment were examined. RT-qPCR analysis indicated that SD significantly attenuated the LPS-induced upregulation of pro-inflammatory cytokines in the BV-2 cells (Fig. 5A). Consistent with the transcriptomic findings, SD also reversed the LPS-induced increases in C3 and MMP9 expression (Fig. 5B and C). Glycolysis provides a rapid source of energy to support microglial proliferation, migration, chemotaxis, and other cellular functions during inflammatory responses (33). To determine whether SD affects microglial metabolic reprogramming, the ECAR and OCR in BV-2 cells were measured following LPS and SD treatment. LPS stimulation significantly increased basal glycolysis and GR, as reflected by elevated ECAR values (Fig. 5D and E). By contrast, LPS significantly reduced basal respiration, maximal respiration and ATP production, as indicated by OCR analysis, compared with untreated control cells (Fig. 5F

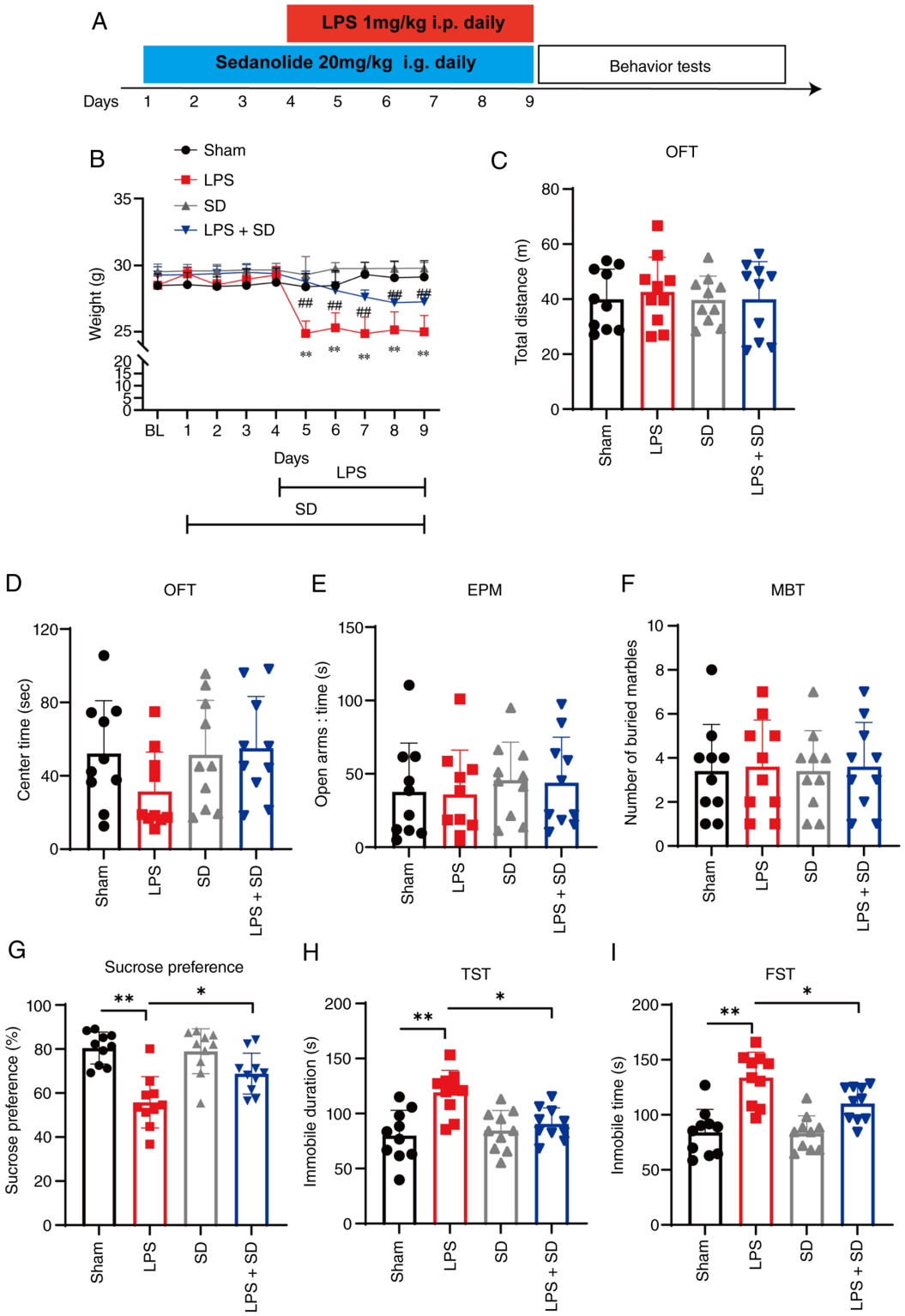

Figure 1. SD alleviates LPS-induced depressive disorder. (A) Schematic diagram of the experimental protocol. (B) Body weight of the LPS mice after SD treatment. Two-way ANOVA and Tukey's multiple comparisons test (n=10 mice per group). (C) Total distance traveled of all the mice in the OFT. Ordinary one-way ANOVA and Tukey's multiple comparisons test (n=10 mice per group). Sham vs. LPS: P=0.9549; sham vs. SD: P>0.9999; LPS vs. LPS + SD: P=0.9561. (D) The stay time in the central area of the OFT. Ordinary one-way ANOVA and Tukey's multiple comparisons test (n=10 mice per group). Sham vs. LPS: P=0.3386; Sham vs. SD P>0.9999; LPS vs. LPS + SD: P=0.2311. (E) The stay time in the open arms in the EPM. Ordinary one-way ANOVA and Tukey's multiple comparisons test (n=10 mice per group). Sham vs. LPS, P=0.9992; sham vs. SD, P=0.9338; LPS vs. LPS + SD, P=0.9363. (F) The number of buried marbles in the MBT. Ordinary one-way ANOVA and Tukey's multiple comparisons test (n=10 mice per group). Sham vs. LPS, P=0.9961; sham vs. SD, P>0.9999; LPS vs. LPS + SD, P>0.9999. (G) The sucrose preference in the sucrose preference test. Ordinary one-way ANOVA and Tukey's multiple comparisons test (n=10 mice per group). Sham vs. LPS, P<0.0001; sham vs. SD, P=0.9864; LPS vs. LPS + SD, P<0.0001. (H) The immobile time in the TST. Ordinary one-way ANOVA and Tukey's multiple comparisons test (n=10 mice per group). Sham vs. LPS, P=0.0003; sham vs. SD, P=0.9458; LPS vs. LPS + SD, P=0.0102. (I) The immobile time in the FST. Ordinary one-way ANOVA and Tukey's multiple comparisons test (n=10 mice per group). Sham vs. LPS, P<0.0001; sham vs. SD P=0.9998; LPS vs. LPS + SD, P=0.0452. Data are presented as the mean ± SEM (n=10). *P<0.05 and **P<0.01. Sham vs. LPS: **P<0.01; LPS vs LPS + SD: $^{\#\#}$P<0.01 in the (B). SD, sedanolide; LPS, lipopolysaccharide; OFT, open field test; EPM, elevated plus maze; FST, forced swimming test; MBT, marble burying test.

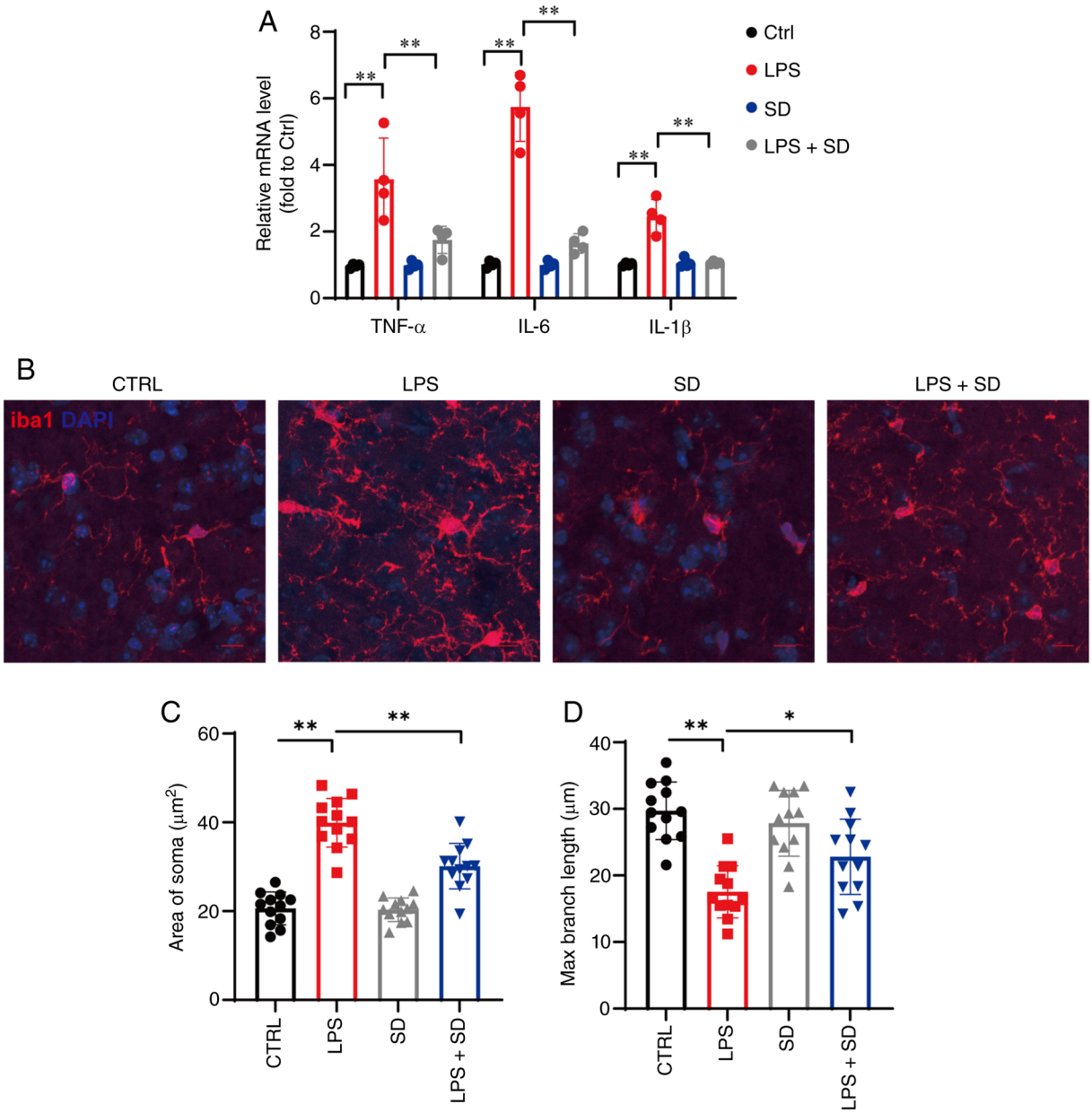

Figure 2. SD releases LPS-induced inflammatory responses. (A) The mRNA levels of TNFα, IL-6 and IL-1β after SD treatment in LPS mice. Two-way ANOVA and Tukey's multiple comparisons test (n=4 mice per group). Ctrl vs. LPS: TNF-a, P<0.0001; IL-6, P<0.0001; IL-1β, P=0.0018; LPS vs. LPS + SD: TNF-a, P<0.0001; IL-6, P<0.0001; IL-1β, P=0.0026. (B) Representative images of immunofluorescence of Iba1 (red). DAPI staining represents for nuclear staining (Blue). Sholl analysis of microglia, (C) Analysis of the area of the soma of microglia. Ordinary one-way ANOVA and Tukey's multiple comparisons test (n=3) mice per group. CTRL vs. LPS, P<0.0001; LPS vs. LPS + SD, P<0.0001. (D) Analysis of the max branch length of microglia. Ordinary one-way ANOVA and Tukey's multiple comparisons test (n=3 mice per group): CTRL vs. LPS, P<0.0001; LPS vs. LPS + SD, P=0.0452. More than 30 images were analyzed for each group. Data are expressed as the mean ± SEM. *P<0.5 and **P<0.01. SD, sedanolide; LPS, lipopolysaccharide.

and G). These findings demonstrate that LPS promotes a metabolic shift toward aerobic glycolysis in microglia, which is closely associated with inflammatory activation. Notably, SD significantly suppressed the LPS-induced increases in basal glycolysis and GR. Moreover, SD restored basal and maximal OCR and improved ATP production in LPS-treated BV-2 cells (Fig. 5D-G). Together, these results indicate that SD attenuates LPS-induced inflammatory activation and metabolic reprogramming in microglia.

To determine whether MMP9 expression is regulated by upstream complement activation, an *in vitro* rescue experiment was performed in BV-2 cells using exogenous recombinant mouse C3a protein. Western blot analysis showed that SD significantly suppressed the LPS-induced increase in MMP9 expression. However, treatment with exogenous C3a effectively reversed this inhibitory effect and restored MMP9 protein expression despite the presence of SD (Fig. 5H and I). These findings provide direct evidence that C3a signaling acts upstream of MMP9 and regulates its expression.

Collectively, the results suggest that the protective effects of SD on neuroinflammation and microglial metabolic reprogramming are closely associated with modulation of the C3a/C3aR signaling pathway and its downstream target, MMP9.

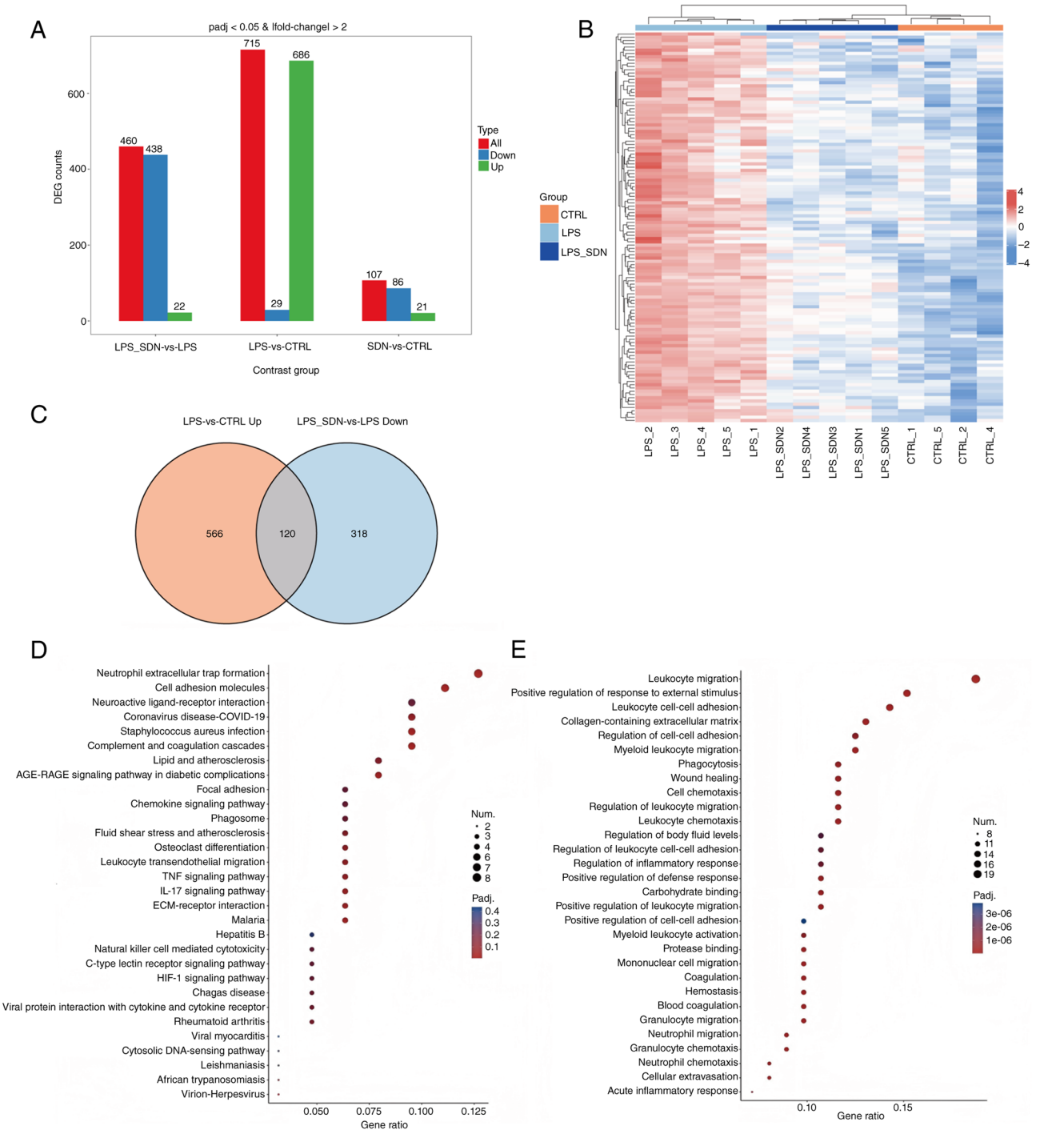

Figure 3. RNA sequencing analysis in the medial prefrontal cortex of LPS-injected mice treated with SDN. (A) The counts of the DEGs correspond to different comparison groups. (B) Heatmap analysis for DEGs correspondingly to different comparison groups. (C) The Venn graph for the upregulation genes in the LPS group vs. the Ctrl group and downregulation genes in the LPS + SDN group vs. LPS group. (D) The Kyoto Encyclopedia of Genes and Genomes analysis for the inner gene of the Venn graph. (E) The Gene Ontology analysis for the inner gene of the Venn graph. LPS, lipopolysaccharide; SDN, sedanolide; DEGs, differentially expressed genes.

Suppressive effects of SD on C3 expression and C3a generation. To determine whether SD regulates C3 expression or its downstream activation through proteolytic cleavage, additional *in vitro* and *in vivo* ELISA assays were performed to quantify C3a levels.

For the *in vitro* assay, BV-2 cells were pretreated with SD (50 μM) for 2 h. Recombinant full-length mouse C3 protein (2 μg/ml) was added to the culture medium 1 h before LPS stimulation to provide an exogenous C3 substrate. Cells were then exposed to LPS (100 ng/ml) to activate the complement cascade. After 24 h, C3a levels in the culture supernatants were measured by ELISA. LPS stimulation significantly increased C3a production, indicating enhanced cleavage of C3 into its active fragment. SD significantly reduced C3a generation in response to LPS. Importantly, this inhibitory effect persisted even in the presence of excess exogenous full-length

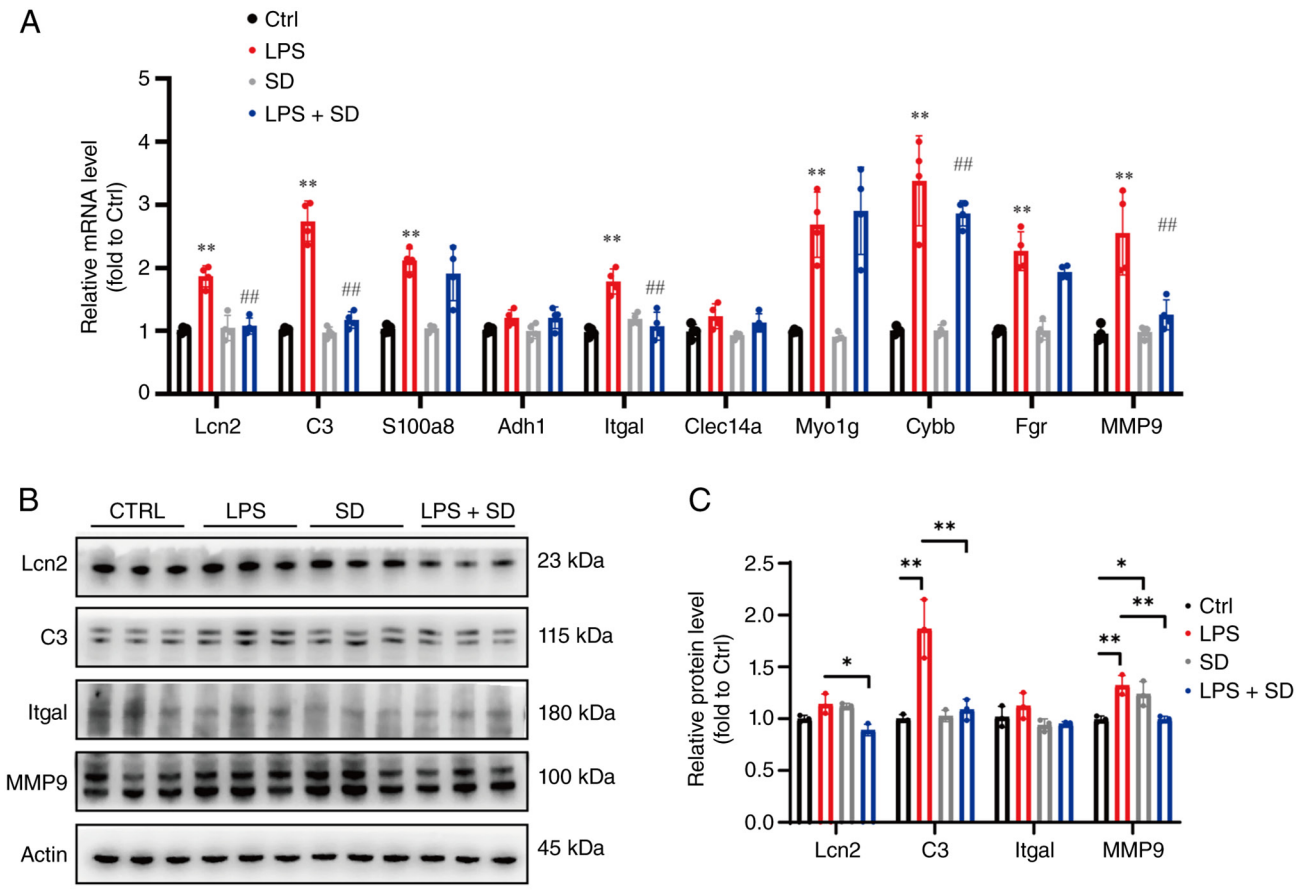

Figure 4. Validation of the RNA-Seq analysis in medial prefrontal cortex. (A) The mRNA levels of the top 10 differentially expressed genes in the inner genes. Two-way ANOVA and Tukey's multiple comparisons test (n=4 mice per group). Ctrl vs. LPS: **P<0.01; LCN2, P<0.0001; C3, P<0.0001; s100a8, P<0.0001; Adh1, P=0.7158; Itgal, P=0.0001; Clec14a, P=0.5539; Myo1g, P<0.0001; Cybb, P<0.0001; Fgr, P<0.0001; and MMP9, P<0.0001. LPS vs. LPS + SD: $^{\#\#}$P<0.01; LCN2, P=0.0002; C3, P<0.0001; s100a8, P=0.6557; Adh1, P>0.9999; Itgal, P=0.0009; Clec14a, P=0.9403; Myo1g, P=0.6125; Cybb, P=0.0267; Fgr, P=0.2757; MMP9, P<0.0001. (B) Representative bands of western blotting for Lcn2, C3, Itgal and MMP9 in mice after LPS and SD treatment. (C) Quantitative analysis of the relative expression of Lcn2, C3, Itgal and MMP9. Two-way ANOVA and Tukey's multiple comparisons test (n=3 mice per group). Ctrl vs. LPS: LCN2, P=0.3075; C3, P<0.0001; Itgal, P=0.5615; and MMP9, P=0.0015. LPS vs. LPS + SD: LCN2, P=0.0197; C3, P<0.0001; Itgal, P=0.1562; and MMP9, P=0.0016. Data are expressed as the mean ± SEM. *P<0.05 and **P<0.01. SD, sedanolide; LPS, lipopolysaccharide.

C3 protein, demonstrating that SD continued to suppress C3a production despite substrate replenishment (Fig. 6A). These findings suggest that SD interferes with the activation process of the complement cascade by inhibiting C3 cleavage rather than simply reducing endogenous C3 availability.

To validate these findings *in vivo*, C3a levels in mPFC tissues from the Ctrl, LPS, SD, and LPS + SD groups were quantified. ELISA analysis showed that 5 consecutive days of LPS administration significantly increased C3a levels in the mPFC, whereas SD treatment significantly attenuated this elevation (Fig. 6B). When considered together with the total C3 and MMP9 expression data presented in Fig. 4, these ELISA results indicate that SD exerts its protective effects by suppressing both C3 expression and the subsequent activation of the C3a signaling pathway.

SD fails to restore LPS-induced depressive disorder after C3aR inhibitor treatment. Complement activation is centered on complement component C3 (C3), which undergoes proteolytic processing to generate several biologically active fragments, including C3a. As an active complement peptide, C3a exerts antimicrobial effects and regulates inflammatory responses .SB290157 trifluoroacetate is a selective antagonist of the C3a receptor (C3aR). Supplementary data showed that SB290157 alone did not significantly affect sucrose preference in LPS-treated mice. Similarly, no significant differences in immobility time during the TST or FST were observed between the LPS and LPS + SB290157 groups (Fig. S2A-C). According to the experimental design shown in Fig. 7A, mice received SB290157 trifluoroacetate (30 mg/kg, i.p.) for two days before SD and LPS administration. SD partially reversed the body weight loss induced by LPS. However, this protective effect was abolished following SB290157 treatment (Fig. 7B). Likewise, no significant difference in sucrose preference was observed between the LPS and LPS + SD + SB290157 groups (Fig. 7C). In addition, SD failed to reduce the LPS-induced increase in immobility time in both the FST and TST when SB290157 administration occurred (Fig. 7D and E). Western blot assays showed that SD mitigated the LPS-induced upregulation of C3 and MMP9. However, this effect was no longer observed in mice treated with SB290157 (Fig. 7F and G).

Together, these findings indicate that the antidepressant-like and anti-inflammatory effects of SD depend on an intact C3a/C3aR signaling pathway, which acts upstream of MMP9 regulation.

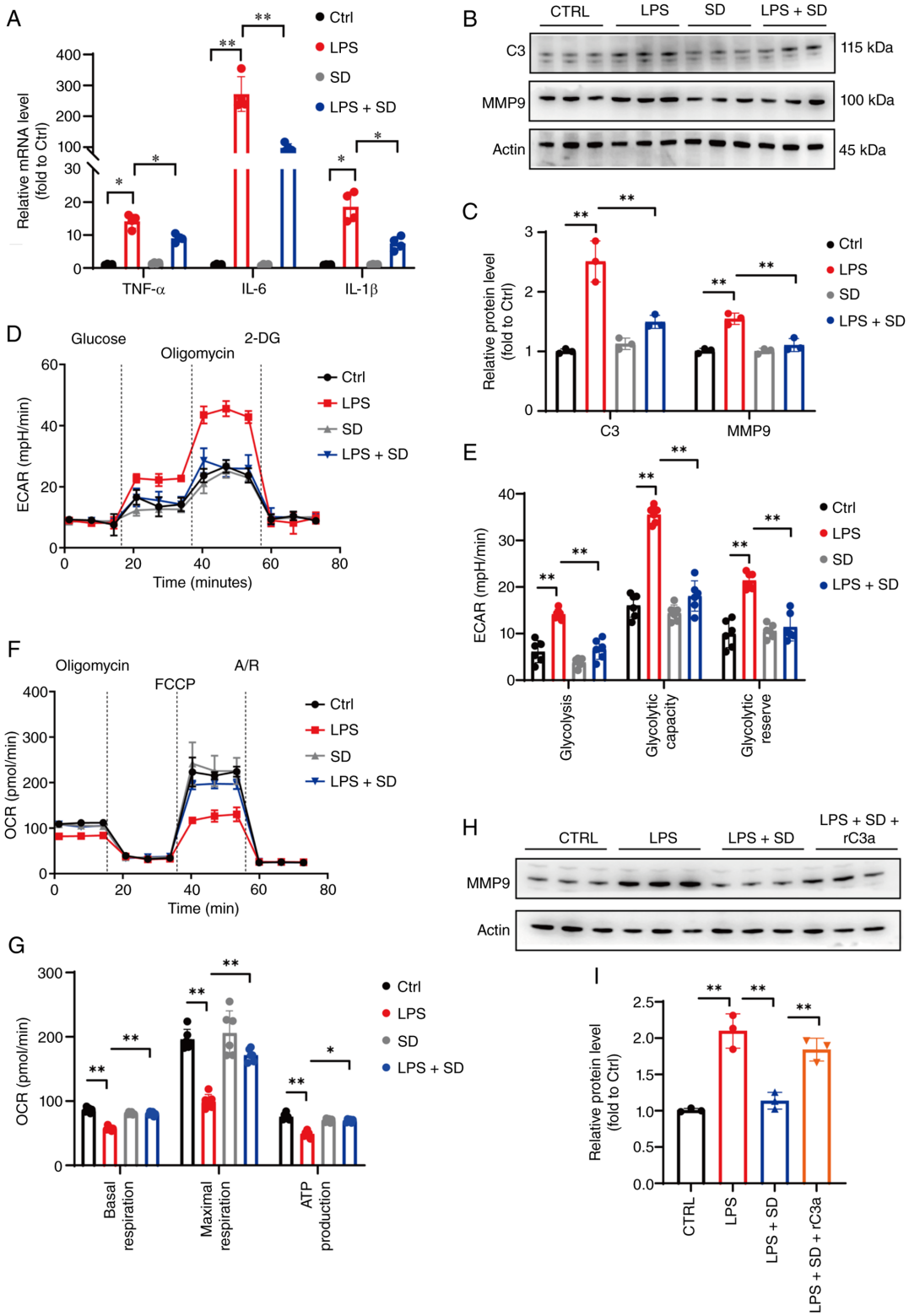

Figure 5. Effect of SD on Complement C3 and aerobic glycolysis in the LPS-induced BV2 cell lines. (A) The mRNA levels of TNFα, IL-6 and IL-1β after LPS and SD treatment in BV-2 cell lines. Two-way ANOVA and Tukey's multiple comparisons test. Ctrl vs. LPS: TNF-a, P=0.021; IL-6, P<0.0001; and IL-1β, P=0.045. LPS vs. LPS + SD: TNF-a, P=0.036; IL-6, P<0.0001 and IL-1β, P=0.042. (B) Representative bands of western blot for C3 and MMP9 in BV2 cell lines after LPS and SD treatment. (C) Quantitative analysis of the relative expression of C3 and MMP9 (n=3). Two-way ANOVA and Tukey's multiple comparisons test, Ctrl vs. LPS: C3, P<0.0001; MMP9, P=0.0013. LPS vs. LPS + SD: C3, P<0.0001; MMP9, P=0.0071. (D and E) The experimental program of the ECAR of BV-2 measured by Seahorse XFe96 Extracellular Flux Analyzer. Two-way ANOVA and Tukey's multiple comparisons test (n=6 dishes), Ctrl vs LPS: Glycolysis, P<0.0001; glycolytic capacity, P<0.0001; GR, P<0.0001. LPS vs. LPS + SD: Glycolysis, P<0.0001; glycolytic capacity, P<0.0001; GR, P<0.0001. (F and G) OCR of BV-2 measured by Seahorse XFe96 Extracellular Flux Analyzer. Ctrl vs LPS: Basal respiration, P=0.0006; maximal respiration, P<0.0001; ATP production, P=0.017. LPS vs. LPS + SD: Basal respiration, P=0.0085; maximal respiration, P<0.0001; ATP production, P=0.0231. (H) Representative bands of western blotting for MMP9 in Bv2 cell lines after administration of exogenous active C3a ligand and SD treatment in the LPS challenge. (I) Quantitative analysis of the relative expression of MMP9 (n=3). Ordinary one-way ANOVA and Tukey's multiple comparisons test, Ctrl vs. LPS: P=0.0001. LPS vs. LPS + SD: P=0.0003. LPS + SD vs. LPS + SD + rC3a: P=0.0023. Data are expressed as the mean ± SEM. *P<0.5 and **P<0.01. SD, sedanolide; LPS, lipopolysaccharide; ECAR, extracellular acidification rate; OCR, oxygen consumption rate; GR, glycolytic reserve; MMP9, matrix metalloproteinase 9.

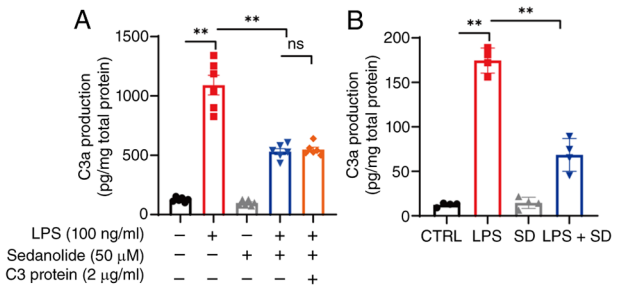

Figure 6. Suppressive effects of SD on C3 activation and C3a generation. (A) C3a level in BV2 cell lines after administration of recombinant full-length mouse C3 protein and SD treatment in the LPS challenge by ELISA assay. Ordinary one-way ANOVA and Tukey's multiple comparisons test (n=6): CTRL vs. LPS, P<0.0001; LPS vs. LPS + SD, P<0.0001; LPS + SD vs. LPS+SD + C3 protein, P=0.9983. (B) The active C3a level in the medial prefrontal cortex tissues after LPS and SD treatment by ELISA assay. Ordinary one-way ANOVA and Tukey's multiple comparisons test (n=4): CTRL vs. LPS, P<0.0001; LPS vs. LPS + SD, P<0.0001. Data are expressed as the mean ± SEM. **P<0.01. LPS, lipopolysaccharide; SD, sedanolide; ns, not significant.

SD partly fails to restore inflammation and aerobic glycolysis in BV-2 cell lines after C3aR inhibitor treatment. The effects of SD on inflammation and aerobic glycolysis were further examined following C3aR inhibition using the BV-2 cell model. SD significantly reduced the LPS-induced increase in pro-inflammatory cytokine expression. However, after treatment with SB290157 trifluoroacetate, SD no longer restored cytokine levels in LPS-stimulated BV-2 cells (Fig. 8A). Similarly, the inhibitory effects of SD on the LPS-induced upregulation of C3 and MMP9 expression were abolished following SB290157 administration (Fig. 8B and C). Metabolic analysis further showed that SD failed to suppress the LPS-induced increases in basal glycolysis and GR, as measured by ECAR, in the presence of SB290157 (Fig. 8D and E). Likewise, in OCR assays, SD lost its ability to restore basal respiration and ATP consumption after C3aR inhibition (Fig. 8F and G). Notably, although SD partially preserved its effect on maximal oxygen consumption, it largely failed to reverse LPS-induced inflammatory responses and metabolic reprogramming following SB290157 treatment.

These findings further demonstrate that the anti-inflammatory and anti-glycolytic effects of SD under LPS stimulation are predominantly mediated through the C3a/C3aR signaling pathway.

Discussion

In the present study, it was demonstrated that SD significantly alleviates LPS-induced depressive-like behaviors by suppressing neuroinflammation and microglial activation in the mPFC. Mechanistically, SD inhibited complement activation by reducing the proteolytic cleavage of C3 into the active fragment C3a, thereby attenuating abnormal microglial aerobic glycolysis. Furthermore, pharmacological blockade of C3aR abolished the protective effects of SD on behavioral deficits, inflammatory responses and metabolic reprogramming. Collectively, these findings indicate that the antidepressant-like effects of SD are mediated through the C3a/C3aR signaling pathway and support its potential as a therapeutic candidate for neuroinflammation-associated depressive disorders.

SD is a naturally occurring phthalide compound isolated from the seed oil of plants belonging to the Umbelliferae family. Owing to its unique biological properties and potential therapeutic value, SD has attracted considerable research interest in recent decades. Previous studies have demonstrated that SD possesses a wide range of pharmacological activities, including anti-inflammatory, hepatoprotective, antitumor and cardioprotective effects against myocardial injury (34). Its antitumor activity has been attributed to multiple mechanisms, including the regulation of cellular autophagy and enhancement of antioxidant defenses. Notably, SD has been shown to increase cellular resistance to oxidative stress through activation of the Kelch-like ECH-associated protein 1 (KEAP1)-NFE2L2 signaling pathway (35). In addition, SD exerts anti-inflammatory effects by suppressing inflammatory signaling pathways, modulating downstream proteins expression, and interfering with the activity of several inflammation-related targets, including COX-2, ERK2, PKC, PI3Kα, PI3Kγ, JAK1, JAK2, JAK3, IKK β and TNF α (36).

In the present study, it was demonstrated that SD significantly alleviates LPS-induced depressive-like behavior. In studies using systemic LPS-induced depression models, it is important to distinguish true antidepressant-like effects from nonspecific improvements in sickness-related behaviors, such as malaise, weight loss, reduced activity, or physical exhaustion. In the present study, neither repeated LPS administration nor SD treatment significantly affected total locomotor activity in the OFT. This essential baseline validation shows that the mice retained fully intact voluntary locomotor capacity at the time of evaluation. Therefore, the prolonged immobility in the TST and FST, together with the anhedonic behavior in the SPT, truly reflects psychological behavioral despair and emotional deficits rather than debilitating physical fatigue (Fig. 1G and H). By selectively reversing these core emotional and motivational deficits while leaving basal movement unchanged, SD demonstrates a specific and genuine antidepressant-like therapeutic profile.

Intriguingly, although SD strongly corrected depression-related indexes, it did not produce noticeable changes in anxiety-related parameters, as shown by the unchanged center stay time in the OFT and the open-arm exploration time in the EPM. This clear phenotypic dissociation was attributed to the chronological design and circuit specificity of the present paradigm. Because the depressive-like phenotypic deficits represented the most reliable and prominent readouts in this model, mechanistic investigation focused on how SD alleviates depression-related neuroinflammation and metabolic reprogramming through the C3a/C3aR axis. Whether SD also has anti-anxiety efficacy in a dedicated anxiety-dominant paradigm remains to be determined.

The complement system can be activated through the classical, lectin, or alternative pathways. These pathways converge at complement C3, a central mediator of the complement cascade, which is cleaved into two biologically active fragments: C3a, a potent anaphylatoxin, and C3b, which promotes further complement activation (8). Following its release, C3a acts as a chemoattractant and binds to the C3aR expressed on various cell types, including microglia. C3aR is a G protein-coupled

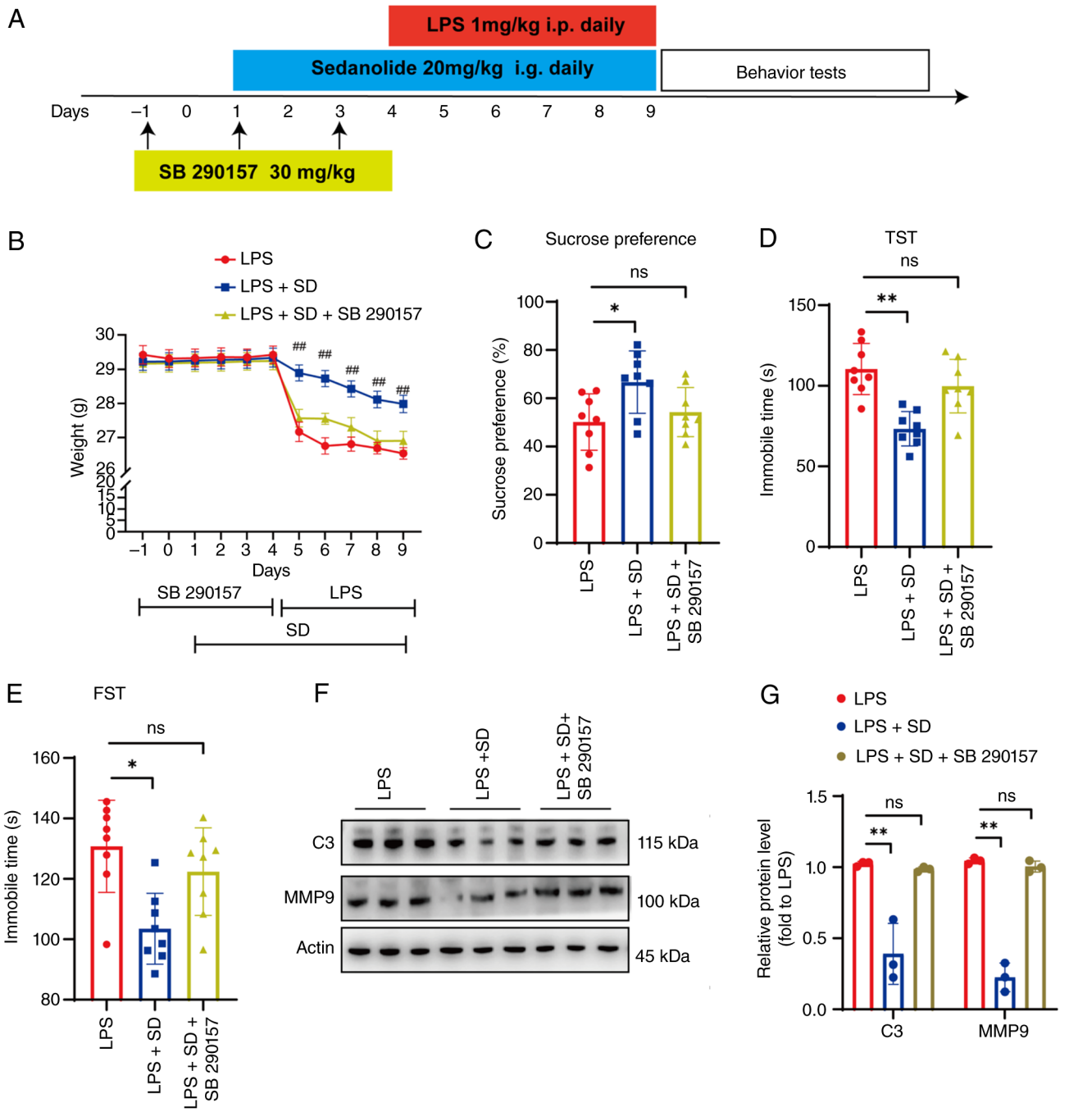

Figure 7. SD fails to restore LPS-induced depressive disorder in the injection of a C3a receptor inhibitor. (A) Schematic diagram of the experimental protocol. (B) Body weight of the LPS mice after SD and SB 290157 treatment. Two-way ANOVA and Tukey's multiple comparisons test, LPS vs. LPS + SD: 5, P<0.0001; 6, P<0.0001; 7, P<0.0001; 8, P=0.0002; 9, P=0.0002. (C) The sucrose preference in the sucrose preference test. Ordinary one-way ANOVA and Tukey's multiple comparisons test (n=8 mice per group). LPS vs. LPS + SD, P=0.0257; LPS + SD vs. LPS + SD + SB 290157, P=0.7655. (D) The immobile time in the TST. Ordinary one-way ANOVA and Tukey's multiple comparisons test (n=8 mice per group): LPS vs. LPS + SD, P=0.0001; LPS + SD vs. LPS + SD + SB 290157, P=0.3311. (E) The immobile time in the FST. Ordinary one-way ANOVA and Tukey's multiple comparisons test (n=8 mice per group). LPS vs. LPS + SD, P=0.0022; LPS + SD vs. LPS+SD+SB 290157, P=0.4642. (F) Representative bands of western blotting for C3 and MMP9 in LPS mice after SD and SB 290157 treatment. (G) Quantitative analysis of the relative expression of C3 and MMP9. Two-way ANOVA and Tukey's multiple comparisons test (n=3 mice per group), LPS vs. LPS + SD: C3, P<0.0001; MMP9, P<0.0001. LPS + SD vs. LPS + SD + SB 290157: C3, P=0.8865; MMP9, P=0.8728. Data are presented as the mean ± SEM. *P<0.5 and **P<0.01. LPS vs. LPS + SD: $^{\#\#}$P<0.01. LPS, lipopolysaccharide; SD, sedanolide; TST, tail suspension test; FST, forced swimming test; ns, not significant.

receptor that undergoes conformational changes upon ligand binding, leading to activation of intracellular G proteins, primarily the Gαi and Gαq subunits (37). Activation of C3aR initiates several downstream signaling pathways, including the phospholipase C, MAPK/ERK, PI3K/Akt and NF-κB pathways (38). Through coordinated signaling involving PKC and PI3K, NF-κB becomes activated and translocates from the cytoplasm to the nucleus (39). Nuclear NF-κB subsequently binds to regulatory regions within the MMP9 promoter, thereby promoting MMP9 transcription and protein synthesis.

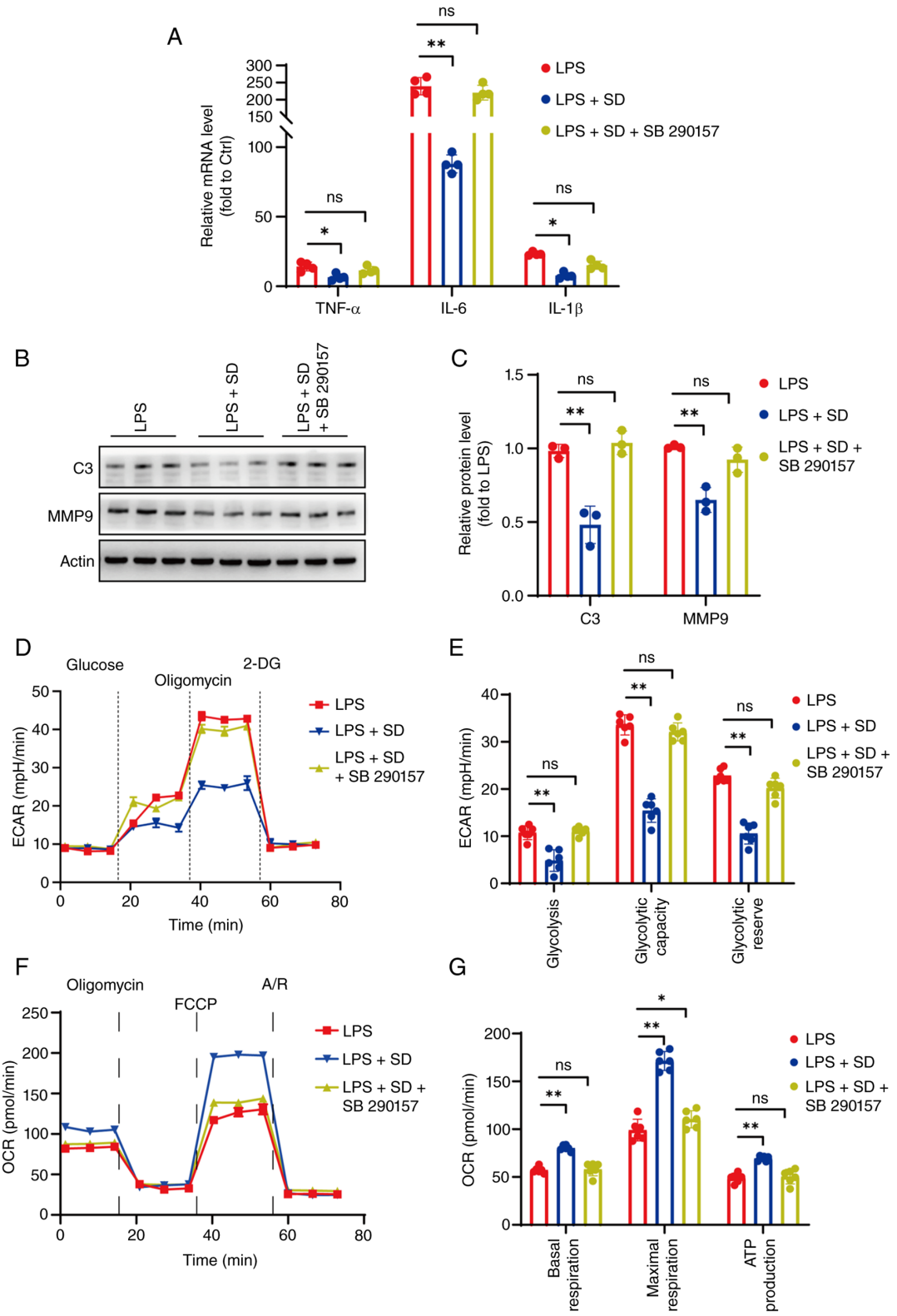

Figure 8. SD partly fails to restore inflammation and aerobic glycolysis in BV-2 cell lines after C3aR inhibitor treatment. (A) The mRNA levels of TNFα, IL-6 and IL-1β after SD and SB 290157 treatment in LPS-induced BV-2 cell lines. Two-way ANOVA and Tukey's multiple comparisons test, LPS vs. LPS + SD: TNF-a, P=0.034; IL-6, P<0.0001; and IL-1β, P=0.041. LPS + SD vs. LPS + SD + SB 290157: TNF-a, P=0.9388; IL-6, P=0.0736; and IL-1β, P=0.5727. (B) Representative bands of western blot for C3 and MMP9 after SD and SB 290157 treatment in LPS-induced BV-2 cell lines. (C) Quantitative analysis of the relative expression of C3 and MMP9 (n=3). Two-way ANOVA and Tukey's multiple comparisons test, LPS vs. LPS + SD: C3, P<0.0001; MMP9, P=0.0004. LPS + SD vs. LPS + SD + SB 290157: C3, P=0.6908; MMP9, P=0.4098. (D and E) The experimental program of the ECAR of BV-2 was measured by Seahorse XFe96 Extracellular Flux Analyzer. Two-way ANOVA and Tukey's multiple comparisons test (n=6 dishes), LPS vs. LPS + SD: Glycolysis, P<0.0001; glycolytic capacity, P<0.0001; GR, P<0.0001. LPS + SD vs. LPS + SD + SB 290157: Glycolysis, P=0.9526; glycolytic capacity, P=0.3825; GR, P=0.0556. (F and G) OCR of BV-2 measured by Seahorse XFe96 Extracellular Flux Analyzer. LPS vs. LPS + SD: Basal respiration, P=0.0006; Maximal respiration, P<0.0001; ATP production, P=0.017. LPS + SD vs. LPS + SD + SB 290157: Basal respiration, P=0.9748; Maximal respiration, P=0.0233; ATP production, P=0.9301. Data are expressed as the mean ± SEM. *P<0.5 and **P<0.01. LPS, lipopolysaccharide; SD, sedanolide; ECAR, extracellular acidification rate; OCR, oxygen consumption rate; GR, glycolytic reserve; ns, not significant.

Cells initially synthesize MMP9 as an inactive zymogen, pro-MMP9, which undergoes extracellular proteolytic processing by enzymes such as plasmin or activated MMPs to generate enzymatically active MMP9. To delineate the molecular sequence underlying the effects of SD, complementary biochemical analyses and *in vitro* ligand-replenishment experiments were conducted to define the relationship between complement activation and MMP9. This integrated approach enabled us to distinguish the effects of SD at multiple levels of the signaling cascade, including total C3 expression, C3 activation through C3a generation, and downstream C3aR-dependent signaling.

At both the transcriptional and protein levels, the present transcriptomic analyses (Fig. 3), together with subsequent western blot validation (Fig. 4), demonstrated that SD suppresses the expression of full-length C3 in both mPFC tissue and BV-2 microglial cells. Specifically, SD reduced C3 transcription and translation, indicating that it decreases the overall availability of C3 and thereby limits the upstream substrate pool required for complement activation. To determine whether SD also regulates complement activation independently of its effects on total C3 expression, *in vitro* substrate-replenishment ELISA assays were performed. Remarkably, supplementation with excess recombinant full-length C3 protein, provided as an exogenous substrate for cleavage, failed to restore C3a generation in SD-pretreated cells, and SD continued to markedly suppress C3a production (Fig. 6). These findings indicate that the actions of SD extend beyond the inhibition of C3 expression and include suppression of the proteolytic activation process responsible for generating biologically active C3a. Consistent with these *in vitro* observations, *in vivo* ELISA analyses further demonstrated that SD significantly reduced active C3a accumulation in mPFC tissue (Fig. 6).

The relationship between complement activation and MMP9 expression was next examined. MMP9 is a zinc-dependent endopeptidase that plays a critical role in inflammatory responses and extracellular matrix remodeling (40). To determine whether MMP9 is regulated downstream of C3a signaling, SD-pretreated, LPS-stimulated BV-2 cells were treated with exogenous recombinant C3a. Western blot analysis showed that exogenous C3a effectively reversed the inhibitory effect of SD and restored MMP9 protein expression (Fig. 5H and I). This gain-of-function experiment provides direct evidence that C3a signaling acts upstream of MMP9. Collectively, these findings support a sequential signaling cascade in which LPS stimulation increases C3 expression and promotes C3 cleavage, leading to elevated C3a production. C3a subsequently activates C3aR signaling, which induces MMP9 expression and contributes to microglial activation and neuroinflammatory responses. SD interrupts this cascade by suppressing both C3 expression and C3 activation, thereby limiting downstream C3a/C3aR signaling and MMP9 induction.

Glycolysis plays a critical role in regulating neuroinflammation. Under inflammatory and stress conditions, microglia undergo metabolic reprogramming and shift from mitochondrial oxidative phosphorylation to aerobic glycolysis (27). Previous studies have showed that glycolytic metabolites promote the production of pro-inflammatory cytokines, including TNF-α, IL-6 and IL-1β. In addition, inhibition of PKM2-dependent aerobic glycolysis reduces microglial C1q, TNF-α and IL-1α levels, leading to decreased C3 expression (41). Transcriptomic analyses of C3aR-positive microglia in APP-KI rats have further demonstrated metabolic alterations characterized by increased HIF-1 signaling and dysregulated lipid metabolism compared with the wild-type controls. Consistent with these findings, Alzheimer's disease has been associated with activation of the C3aR/HIF-1α signaling axis, which influences lipid homeostasis and microglial metabolism (12). Consistent with previous reports, the present Seahorse extracellular flux analyses showed that LPS stimulation significantly increased basal glycolysis and glycolytic capacity while reducing basal respiration and ATP production. SD effectively reversed these metabolic changes by suppressing excessive aerobic glycolysis and restoring mitochondrial oxidative phosphorylation in microglia (Fig. 5D-G).

To determine whether the metabolic effects of SD depend on complement signaling, the selective C3aR antagonist SB290157 was used to block downstream C3a/C3aR signaling. Notably, pharmacological inhibition of C3aR completely abolished the ability of SD to suppress LPS-induced microglial glycolysis and restore ATP production *in vitro* (Fig. 8). These cellular findings were consistent with our *in vivo* results, in which co-administration of SB290157 eliminated the beneficial effects of SD on behavioral despair, anhedonia, and neuroinflammation in the prefrontal cortex (Fig. 7). Importantly, the additional control experiments of the present study demonstrated that SB290157 alone did not significantly alter sucrose preference or immobility time in LPS-treated mice (Fig. S2). These findings indicate that inhibition of C3aR is not sufficient to directly modify the depressive-like phenotype under the present experimental conditions. Rather, the C3a/C3aR signaling pathway appears to be essential for the therapeutic actions of SD. Collectively, these results demonstrate that the anti-inflammatory, anti-glycolytic, and antidepressant-like effects of SD are dependent on an intact C3a/C3aR signaling axis.

Several methodological and conceptual limitations should be considered when interpreting the findings of the present study. First, all behavioral and biochemical experiments were performed exclusively in male mice. Because sex differences can substantially influence microglial responses and complement system activation during inflammatory challenges, the absence of female animals limits the generalizability of the prsent findings. Future studies should therefore validate these results in female cohorts. Second, the 5-day LPS paradigm used in the present study represents a subacute model of neuroinflammation-induced depressive-like behavior. Although this model is well established and highly reproducible for investigating inflammation-related mechanisms, it does not fully capture the complex, chronic, and multifactorial nature of human MDD. Notably, within this experimental paradigm, SD effectively improved behavioral despair and anhedonia but did not significantly alter anxiety-related behaviors in the OFT or EPM. This behavioral dissociation suggests that the present model predominantly induces depressive-like rather than anxiety-like phenotypes. Whether SD exerts anxiolytic effects under dedicated anxiety models requires further investigation. Third, mechanistic studies

were conducted primarily in the BV-2 microglial cell line. Although BV-2 cells provide a convenient and reproducible model for examining inflammatory and metabolic responses, they are immortalized cells and therefore do not fully replicate the physiological characteristics of primary microglia or tissue-resident brain immune cells. Consequently, future studies using primary microglia and additional *in vivo* approaches will be necessary to further validate the mechanisms identified in the present study. Future studies using primary microglia or *in vivo* cell-sorting approaches are needed to further validate the metabolic alterations identified in the present study. Fourth, although pharmacological loss-of-function experiments using SB290157 and *in vitro* ligand-replenishment assays strongly support the dependence of SD on C3a/C3aR signaling, it was not directly examined whether SD physically interacts with complement components or other molecular targets within this pathway. Therefore, additional target-validation studies, including surface plasmon resonance, cellular thermal shift assays, and other biochemical binding approaches, will be required to define the direct molecular targets and mechanism of action of SD.

In conclusion, the present study investigated the therapeutic effects of SD and its underlying mechanisms in an LPS-induced mouse model of depressive-like behaviors. The results of the present study demonstrate that SD effectively alleviates behavioral despair and anhedonia induced by systemic inflammatory challenge. Mechanistically, LPS activates complement C3 signaling, promotes MMP9 expression, and induces microglial metabolic reprogramming characterized by enhanced aerobic glycolysis. SD suppresses C3 activation, reduces downstream MMP9 expression, attenuates neuroinflammation, and restores microglial metabolic homeostasis. Importantly, pharmacological inhibition of C3aR completely abolishes the beneficial effects of SD on depressive-like behaviors, neuroinflammatory responses, and metabolic dysfunction.

Collectively, these findings indicate that SD mitigates neuroinflammation-associated depressive-like behaviors through a mechanism that depends on the C3a/C3aR signaling pathway.

Acknowledgements

The authors express gratitude to Dr Sanhua Fang and Dr Jiajia Wang of the Core Facilities at Zhejiang University School of Medicine for their invaluable technical assistance.

Funding

The present study was supported by the National Natural Science Foundation of China (grant no. 82001424).

Availability of data and materials

The sequencing data generated in the present study may be found in the NCBI Gene Expression Omnibus database under the accession number GSE335983 or at the following URL: https://www.ncbi.nlm.nih.gov/geo/query/acc.cgi?acc=GSE335983. The other data generated in the present study may be requested from the corresponding author.

Authors' contributions

YC and SL conceptualized the study. SL and FL conducted statistical analysis, ImageJ quantification and GO/KEGG analysis, and interpreted the results. SL, FL, NC and GS performed animal experiments, cell culture, molecular biology experiments, immunostaining and behavioral tests. SL, FL, NC and GS collected, organized, verified and managed the experimental datasets and raw data. SL and YC edited the manuscript and prepared the original draft. YC and SL confirm the authenticity of all the raw data. YC wrote, reviewed and edited the manuscript, supervised the study, conducted project administration and acquired funding. All authors read and approved the final version of the manuscript.

Ethics approval and consent to participate

All animal experiments were performed in accordance with the animal testing guidelines of Zhejiang University and the Guide for the Care and Use of Laboratory Animals published by the National Institutes of Health. Experimental protocols were reviewed and approved by the Animal Care and Use Committee of Zhejiang University (Hangzhou, China; approval no. ZJU20220307). The supplementary *in vivo* receptor-antagonism control procedures (LPS + SB290157 cohort) were independently authorized and approved by Animal Experimental Ethical Inspection of the Sir Run Run Shaw Hospital, Zhejiang University School of Medicine (Hangzhou, China; approval no. SRRSH2026-0041).

Patient consent for publication

Not applicable.

Competing interests

The authors declare that they have no competing interests.

References

1. Mathers CD and Loncar D: Projections of global mortality and burden of disease from 2002 to 2030. PLoS Med 3: e442, 2006.
2. Smith RS: The macrophage theory of depression. Med Hypotheses 35: 298-306, 1991.
3. Ge C, Chen W, Zhang L, Ai Y, Zou Y and Peng Q: Chemogenetic activation of the HPC-mPFC pathway improves cognitive dysfunction in lipopolysaccharide -induced brain injury. Theranostics 13: 2946-2961, 2023.
4. Rezaei S, Prévot TD, Vieira E and Sibille E: LPS-induced inflammation reduces GABAergic interneuron markers and brain-derived neurotrophic factor in mouse prefrontal cortex and hippocampus. Brain Behav Immun Health 38: 100761, 2024.
5. Maziz MNH, Chakravarthi S, Aung T, Htoo PM, Shwe WH, Gupalo S, Udayah MW, Singh H, Kabir MS, Thangarajan R and Kodali M: Microglia-mediated neuroinflammation through phosphatidylinositol 3-kinase signaling causes cognitive dysfunction. Int J Mol Sci 26: 7212, 2025.
6. Arioz BI, Tastan B, Tarakcioglu E, Tufekci KU, Olcum M, Ersoy N, Bagriyanik A, Genc K and Genc S: Melatonin attenuates LPS-induced acute depressive-like behaviors and microglial NLRP3 inflammasome activation through the SIRT1/Nrf2 pathway. Front Immunol 10: 1511, 2019.
7. Korol' SA: Complement system. Fiziol Zh 23: 408-416, 1977 (In Ukrainian).

8. Stephan AH, Barres BA and Stevens B: The complement system: An unexpected role in synaptic pruning during development and disease. Annu Rev Neurosci 35: 369-389, 2012.
9. Zhou R, Chen SH, Zhao Z, Tu D, Song S, Wang Y, Wang Q, Feng J and Hong JS: Complement C3 enhances LPS-elicited neuroinflammation and neurodegeneration via the Mac1/NOX2 pathway. Mol Neurobiol 60: 5167-5183, 2023.
10. Kolev M, Le Friec G and Kemper C: Complement-tapping into new sites and effector systems. Nat Rev Immunol 14: 811-820, 2014.
11. Hess C and Kemper C: Complement-mediated regulation of metabolism and basic cellular processes. Immunity 45: 240-254, 2016.
12. Gedam M, Comerota MM, Propson NE, Chen T, Jin F, Wang MC and Zheng H: Complement C3aR depletion reverses HIF-1α-induced metabolic impairment and enhances microglial response to Aβ pathology. J Clin Invest 133: e167501, 2023.
13. Sun XP, Shi Z, Pan RL, Qin C, Zhang YL, Li YH, Qu LN, Li TF and Liu XM: Antidepressant-like effects and mechanism of action of SYG in depression model in rats. Neuro Endocrinol Lett 35: 129-136, 2014.
14. Wei Q, Yang J, Li L, Su Y and Wang A: Novel phthalide dimers from the aerial parts of Ligusticum sinense Oliv cv. Chaxiong. Fitoterapia 137: 104174, 2019.
15. Chen Y, Cheng Q, Lv S, Kang Z and Zeng S: Advances in the phytochemistry and pharmacology of plant-derived phthalides. Heliyon 9: e22957, 2023.
16. Ling J, Deng W, Zhang J and Yang F: The protective effect of Chuanxiong Oil on focal cerebral reperfusion injury in rat. Pharmacol Clin Chin Mat Med 24: 39-41, 2008 (In Chinese).
17. Fan Y, Wang J, Jian J, Wen Y, Li J, Tian H, Crommen J, Bi W, Zhang T and Jiang Z: High-throughput discovery of highly selective reversible hMAO-B inhibitors based on at-line nano-fractionation. Acta Pharm Sin B 14: 1772-1786, 2024.
18. Li S, Zhuge A, Chen H, Han S, Shen J, Wang K, Xia J, Xia H, Jiang S, Wu Y and Li L: Sedanolide alleviates DSS-induced colitis by modulating the intestinal FXR-SMPD3 pathway in mice. J Adv Res 69: 413-426, 2025.
19. Singh P and Mohanty B: Mechanisms of repetitive LPS exposure-induced toxicity in murine model via toll-like receptor 4 mediated NF-κB/NLRP3/COX-2 signalling: An in vivo and in silico analysis. Food Chem Toxicol 206: 115785, 2025.
20. Wang X, Weng G, Gao Y, Wang Y and Zhang C: Quercetin ameliorates chronic restraint stress- and LPS-induced anxiety-like behaviors by modulating neuroinflammation in the lateral hypothalamus. Psychopharmacology (Berl) 242: 2063-2076, 2025.
21. Hu Q, Cai H, Ke X, Wang H, Zheng D, Chen Y, Wang Y and Chen G: The lateral septum partakes the regulation of propofol-induced anxiety-like behavior. Eur J Pharmacol 977: 176756, 2024.
22. Chen Y, Zheng D, Wang H, Zhang S, Zhou Y, Ke X and Chen G: Lipocalin 2 in the paraventricular thalamic nucleus contributes to DSS-induced depressive-like behaviors. Neurosci Bull 39: 1263-1277, 2023.
23. Livak KJ and Schmittgen TD: Analysis of relative gene expression data using real-time quantitative PCR and the 2(-Delta Delta C(T)) method. Methods 25: 402-408, 2001.
24. Song S, Zhao W, Ji Y, Huang Q, Li Y, Chen S, Yang J and Jin X: SHANK2 protein contributes to sevoflurane-induced developmental neurotoxicity and cognitive dysfunction in C57BL/6 male mice. Anesthesiol Perioper Sci 1: 2, 2023.
25. Zheng XZ, Yu HY, Chen YR and Fang JS: Aucubin mitigates the elevation of microglial aerobic glycolysis and inflammation in diabetic neuropathic pain via aldose reductase. World J Diabetes 16: 103915, 2025.
26. Li S, Liu H, Lv P, Yao Y, Peng L, Xia T, Yan C, Ma Z, Chen ZP, Zhao C and Gu X: Microglia mediate memory dysfunction via excitatory synaptic elimination in a fracture surgery mouse model. J Neuroinflammation 21: 227, 2024.
27. Hu Y, Mai W, Chen L, Cao K, Zhang B, Zhang Z, Liu Y, Lou H, Duan S and Gao Z: mTOR-mediated metabolic reprogramming shapes distinct microglia functions in response to lipopolysaccharide and ATP. Glia 68: 1031-1045, 2020.
28. Kim D, Langmead B and Salzberg SL: HISAT: A fast spliced aligner with low memory requirements. Nat Methods 12: 357-360, 2015.
29. Pertea M, Pertea GM, Antonescu CM, Chang TC, Mendell JT and Salzberg SL: StringTie enables improved reconstruction of a transcriptome from RNA-seq reads. Nat Biotechnol 33: 290-295, 2015.
30. Li B and Dewey CN: RSEM: Accurate transcript quantification from RNA-Seq data with or without a reference genome. BMC Bioinformatics 12: 323, 2011.
31. Love MI, Huber W and Anders S: Moderated estimation of fold change and dispersion for RNA-seq data with DESeq2. Genome Biol 15: 550, 2014.
32. Wang L, Feng Z, Wang X, Wang X and Zhang X: DEGseq: An R package for identifying differentially expressed genes from RNA-seq data. Bioinformatics 26: 136-138, 2010.
33. Li Y, Kong E, Ding R, Chu R, Lu J, Deng M, Hua T, Yang M, Wang H, Chen D, *et al*: Hyperglycemia-induced Sirt3 downregulation increases microglial aerobic glycolysis and inflammation in diabetic neuropathic pain pathogenesis. CNS Neurosci Ther 30: e14913, 2024.
34. Xie Q, Zhang X, Zhao S, Chen S, Liu M, Zhu C, Zhao Y, Gui Y and Ma R: Sedanolide: A review on its chemical compounds, mechanisms and functions. Fitoterapia 185: 106732, 2025.
35. Tabei Y, Abe H, Suzuki S, Takeda N, Arai JI and Nakajima Y: Sedanolide activates KEAP1-NRF2 pathway and ameliorates hydrogen peroxide-induced apoptotic cell death. Int J Mol Sci 24: 16532, 2023.
36. Ma N, Fan S, Li X, *et al*: Screening of anti-inflammatory substances of Chuanxiong Rhizoma and analysis of its mechanism. Chin J Exp Tradit Med Formulae 24: 140-146, 2018 (In Chinese).
37. Gedam M and Zheng H: Complement C3aR signaling: Immune and metabolic modulation and its impact on Alzheimer's disease. Eur J Immunol 54: e2350815, 2024.
38. Yan H, Zhang JL, Leung KT, Lo KW, Yu J, To KF and Kang W: An update of G-protein-coupled receptor signaling and its deregulation in gastric carcinogenesis. Cancers (Basel) 15: 736, 2023.
39. Rothwarf DM and Karin M: The NF-kappa B activation pathway: A paradigm in information transfer from membrane to nucleus. Sci STKE 1999: RE1, 1999.
40. Wang Y, Jiao L, Qiang C, Chen C, Shen Z, Ding F, Lv L, Zhu T, Lu Y and Cui X: The role of matrix metalloproteinase 9 in fibrosis diseases and its molecular mechanisms. Biomed Pharmacother 171: 116116, 2024.
41. Li X, Zhou R, Peng H, Peng J, Li Q and Mei M: Microglia PKM2 mediates neuroinflammation and neuron loss in mice epilepsy through the astrocyte C3-neuron C3R signaling pathway. Brain Sci 13: 262, 2023.